Ruthenocenoporphyrinoids - π-Conjugation Transmitted Across 1,3-Substituted Ruthenocene

Anna Berlicka*, Aleksandra Walczak, Michał J. Białek, Katarzyna Ślepokura, Piotr J. Chmielewski, and Lechosław Latos-Grażyński*

[a] Dr. Anna Berlicka, Aleksandra Walczak, Dr. Michał J. Białek, , Dr. Katarzyna Ślepokura, Prof. Piotr J. Chmielewski, Prof. Lechosław Latos-Grażyński
Department of Chemistry
University of Wrocław
14 F. Joliot-Curie, 50-383 Wrocław, Poland
E-mail: anna.berlicka@uwr.edu.pl, lechoslaw.latos-grazynski@uwr.edu.pl

Supporting information for this article is given via a link at the end of the document.

Abstract: Synthesis of ruthenocenoporphyrinoids, wherein the $[RuCp^*]^+$ moiety coordinates to the cyclopentadienyl π-surface of the 21-carba-23-selenaporphyrin macrocyclic platform has been developed. The specific electronic ruthenocene-macrocycle communication is observed. The macrocyclic ring current is maintained despite the strong π-conjugation in the cyclopentadienyl ring of the ruthenocene fragment. The theoretical data are consistent with magnetic properties reflected by ^{1}H NMR spectra. DFT-optimized molecular models were used to evaluate the NICS 2D maps and EDDB plots. These data gave an insight into the aromaticity and effectiveness of π-conjugation across 1,3-substituted ruthenocene in obtained hybrid molecules.

Introduction

Porphyrins and their analogous are excellent scaffolds for advanced investigation of the macrocyclic π aromaticity. The aromaticity of various porphyrinoid systems has been extensively investigated.[1] Several factors, such as the molecular framework's topology, the molecule's conformation, metal coordination in the inner core, and tautomerism, can determine their π-electron conjugation.

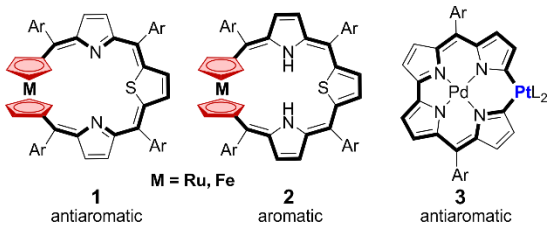

Figure 1. π-Delocalization through metallocenes (**1**, **2**) and the metal center (**3**).

The macrocycles combining the structural features of *ansa*-metallocenes and heteroporphyrin were obtained. The reported ferroceno- and ruthenocenoporphyrinoids provide evidence for direct transmission of π-electron conjugation across a *d*-electron ferrocene and ruthenocene, respectively (**1**, **2**; Figure 1).[2,3] In the case of ruthenocenothiaporphyrin and ruthenocenoporphyrin, the corresponding macrocyclic antiaromaticity and aromaticity observed for the same number of π electrons were controlled by the mutual orientation of the cyclopentadienyl (Cp) rings.[3] Recently, the effective π-conjugation through *d*-orbitals of the metal center, resulting in the antiaromatic character of the platinacorrole complex, has also been documented (**3**, Figure 1).[4]

The metallocene unit can be incorporated into the macrocyclic platform in three different modes: 1,1'; 1,2 and 1,3, as shown in Figure 2. To date, several bridged 1,1'-metallocene macrocycles have been reported. Except for a few examples involving the porphyrinoids **1** and **2**,[2,3,5] macrocyclic π-conjugation is impossible due to structural and/or conformational features.[6] On the other hand, metallocenes that are 1,2- and 1,3-disubstituted and incorporated into a cyclic framework (Figure 2) are exceedingly uncommon.[7]

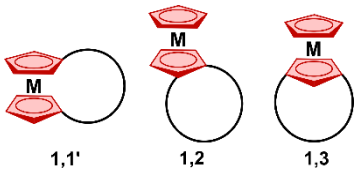

Figure 2. Feasible motifs of metallocene incorporation into a macrocyclic structure.

The incorporation of metallocene subunits at the 1,2 or 1,3 positions into fully π-conjugated macrocycles is of fundamental importance in determining the overall electronic properties of the created hybrid molecules.[8,9] The recent approach of direct metal π complexation to various oligopyrrolic ligands has been shown to modulate their spectroscopic, redox, optical, and electronic properties. In this approach, a direct coordination of $[RuCp]^+$, $[RuCp^*]^+$ (Cp*, pentamethylcyclopentadienyl), or [Ru(*p*-cymene)]$^+$ fragment to pyrrole π-surface of π-conjugated porphyrins (**4**),[10] porphycenes (**5**)[11] and hexaphyrins[12] has been investigated (Figure 3). In these complexes with a "fused" 1,3-azaruthenocene moiety (**4**, **5**; Figure 3), strong electronic azaruthenocene-macrocycle communication was observed.[10,11] The synthesis of *β,β'*-fused cyclopentenylporphyrins allowed the introduction of a metallocene at the macrocyclic periphery (**6**, Figure 3).[13]

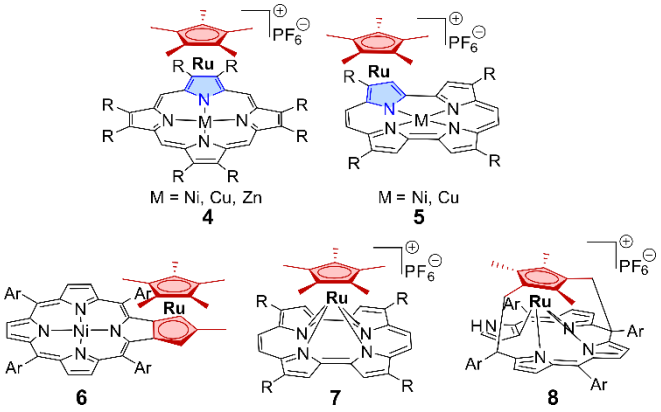

Figure 3. Examples of the coordination motifs of $[RuCp^*]^+$ to porphyrinoids.

A different coordination motif of pentamethylcyclopentadienyl ruthenium cation is represented by "sitting-atop" semisandwich complexes of porphycene **7**,[11] N-fused porphyrin,[14] and N-confused porphyrin **8**,[15] in which a $[RuCp^*]^+$ fragment is accommodated in the central N_3/N_4 core of the macrocycle.

Results and Discussion

Based on the above investigations and a recent study of 21-carbaselenaporphyrinoids **9** and **10** (Schemes 1 and 2),[16] it is assumed that 21-carba-23-selenaporphyrin **9** can serve as a perfect macrocyclic π-conjugated platform for the coordination to a cyclopentadienyl ruthenium fragment, leading to the formation of the 1,3-metallacenoporphyrin hybrid (Figure 2). In contrast to other 21-carbaheteroporphyrins,[17,18] 21-carba-23-selenaporphyrin exists predominantly as a tautomer **9-I** with the tetrahedral C(21) carbon atom (Scheme 1).[16] Importantly, 1,3-metallocenoporphyrin was postulated as an intermediate complex in the synthesis of *meso*-tetraaryl-21-carbaporphyrin.[19]

Herein, we report the synthesis and characterization of ruthenocenoselenaporphyrin **11** and its palladium complex **15**. Importantly, these hybrid carbaporphyrin-ruthenocene molecules indicate the direct transmission of π-electron conjugation across the 1,3-ruthenocene bridge. Significantly, the macrocyclic aromaticity is influenced by protonation or metal coordination in the metallocenoporphyrin cavity.

Treatment of 21-carbaselenaporphyrin **9** or its palladium complex **14** with $[RuCp^*(CH_3CN)_3][PF_6]$ in dichloromethane at 293 K resulted in the η^5-coordination of a $[RuCp^*]^+$ fragment to the cyclopentadiene ring of **9** or **14**. This led to the formation of ruthenocenoporphyrin **11** (Scheme 1) or bimetallic palladium(II) ruthenocenoporphyrin **15** (two stereoisomers, Scheme 2) with yields of 62% and 96%, respectively. Palladium(II) 21-carbaselenaporphyrin **14** was synthesized on an NMR scale by attentive titration of the corresponding 21-carbaselenachlorin complex **13** with a saturated solution of DDQ in [D]chloroform (Scheme 2). Palladium(II) complexes **12** and **13** were obtained in the reaction of 21-carbaselenachlorin **10** with $PdCl_2$ in DMF at reflux with 5% and 39% yields, respectively (Scheme 2; see SI). The selective formation of complex **13** with a yield of 58% was observed in a mixture of $CHCl_3/CH_3CN$ used as a solvent.

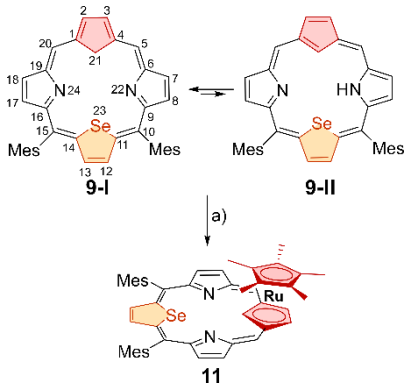

Scheme 1. Synthesis of ruthenocenoporphyrin **11** (conditions a): $[RuCp^*(CH_3CN)_3][PF_6]$ (0.5 equiv), CH_2Cl_2, 293 K.

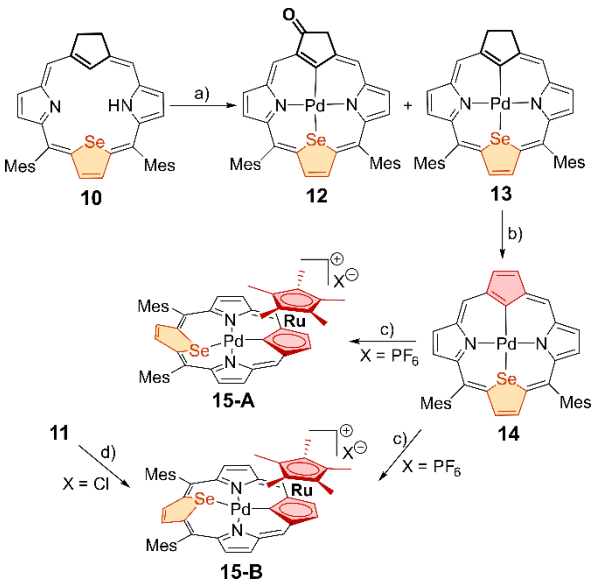

Scheme 2. Synthesis of palladium(II) ruthenocenoporphyrin **15**. Reaction conditions a): $PdCl_2$ (10 equiv), K_2CO_3, DMF, reflux, 10 minutes; b): DDQ, $CDCl_3$ (NMR titration), c): $[RuCp^*(CH_3CN)_3][PF_6]$ (1.1 equiv), CH_2Cl_2, 293 K, and d): $PdCl_2$ (10 equiv), K_2CO_3, $CHCl_3/CH_3CN$, reflux, 10 minutes.

The coordination of the $[RuCp^*]^+$ moiety to the cyclopentadiene ring of **9** has been confirmed by X-ray diffraction studies (Figure 4).[20] The macrocyclic ring adopts a nearly planar conformation. The planes of the macrocyclic cyclopentadienyl and the pentamethylcyclopentadienyl rings are almost parallel (the dihedral angle is equal to 4.5°). The distances between the Cp*, Cp ring planes, and the ruthenium ion are 1.81 and 1.83 Å, respectively. These values are slightly longer than those observed in the corresponding RuCp*-polyarene complexes (ca.

1.80-1.81Å)[21] and RuCp* complexes of *β*-substituted porphyrin and porphycene (ca. 1.78-1.79 Å).[10,11]

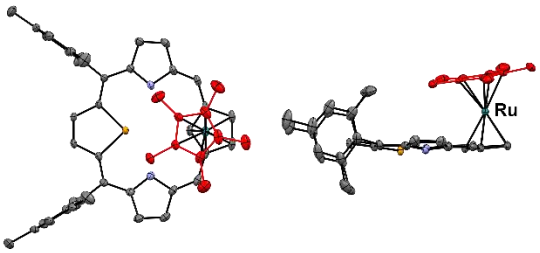

Figure 4. The molecular structure of **11** is presented in two perspectives: a top view (left) and a side view (right). Atoms of pentamethylocyclopentadienyl ring are shown in red. The displacement ellipsoids indicate a 30% probability. Hydrogen atoms, the disorder of Cp*, and mesityl groups have been omitted for clarity.

The molecular structure of **13** exhibits a significant deviation from planarity (Figure 5).[20] This is due to the selenophene ring being tilted at an angle of 38.0° to the macrocyclic plane, defined by four *meso*-carbons. This distortion allows the pyramidal side-on coordination of the palladium(II) ion.

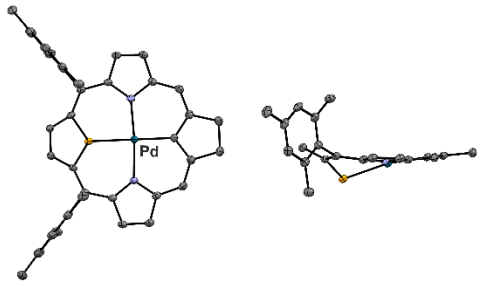

Figure 5. The molecular structure of **13** is presented in two perspectives: a top view (left) and a side view (right). The displacement ellipsoids indicate a 30% probability. Hydrogen atoms have been omitted for clarity.

The electronic spectrum of ruthenocenoselenaporphyrin **11** (blue in Figure 6) displays four bands at 299, 385, 449, and 692 nm. The Soret band at 449 nm is batochromically shifted compared to 21-carbaselenaporphyrin **9** (423 nm, red in Figure 6).[16] The electronic absorption spectrum of **14** shows eight bands from 350 to 790 nm, while the palladium(II) of ruthenocenoselenaporphyrin **15** (mixture of two isomers) demonstrates an entirely different spectrum with three bands at 302, 404, and 497 nm (Figure S31).

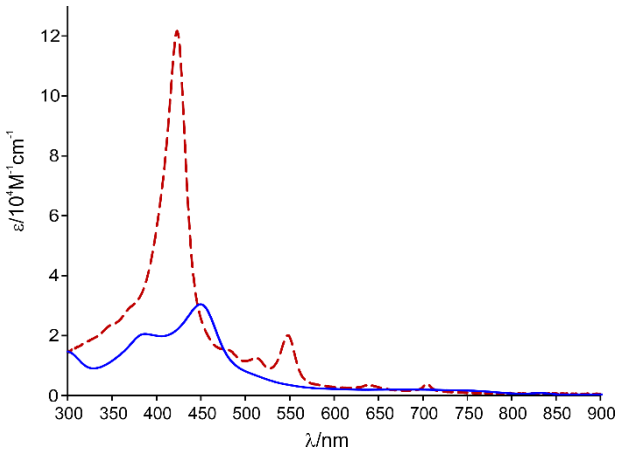

Figure 6. UV/Vis spectra of **9** (dashed red) and **11** (solid blue) in dichloromethane.

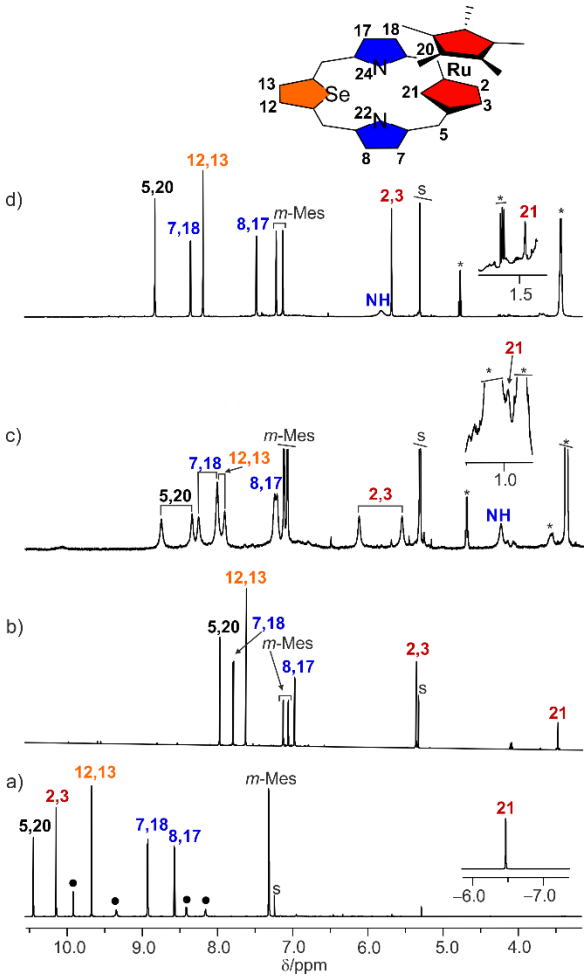

Figure 7. ^{1}H NMR spectra for compounds a) **9-I** (**9-II** shown as black circles, 300 K, [D]chloroform), b) **11** (300 K, [D$_2$]dichloromethane), c) **11-H$^+$** (190 K, [D$_2$]dichloromethane), and d) **11-H$_2^{2+}$** (300 K, [D$_2$]dichloromethane). *o,p*-Methyl range is omitted (see SI for details). Inset at trace d) presents the numbering of proton positions.

The ^{1}H NMR spectrum of the ruthenium(II) π-complex of 21-carba-23-selenaporphyrin **11** indicates its C_s symmetry (Figure 7b). The resonances of the external macrocyclic ring protons are relocated upfield compared to those of parent macrocycle **9** (Figure 7a). The external *meso*-H and selenophene H(12,13) are detected at 7.96 and 7.61 ppm, respectively. The β protons of the pyrrole rings H(7,18) and H(8,17) produce two doublets observed at 7.78 and 6.97 ppm, correspondingly. The outer protons H(2,3) of cyclopentadiene give a doublet at 5.35 ppm, resulting from the scalar coupling with the inner H(21). The inner H(21) proton shows a significant relocation to 3.47 ppm, in contrast to **9** (**9-I**: −6.53 ppm; **9-II**: −4.17 ppm),[16] however similar to the chemical shifts observed for ruthenocene (δ = 4.52 ppm).[22] The positions of the signals indicate a weakening of the diatropic ring current due to the η^5-π bonding of $[RuCp^*]^+$ fragment to the cyclopentadiene ring of **9**. Notably, the ^{13}C chemical shifts detected for the cyclopentadiene carbon atoms C(1,4), C(2,3), and C(21) of **11** at 89.1, 82.4, and 77.3 ppm, respectively, clearly indicate coordination of the carbaselenaporphyrin platform to the $[RuCp^*]^+$ moiety (for ruthenocene and its substituted derivatives δ = 70.0–91.0 ppm).[23]

Gradual acidification of compound **11** with a fluoroboric acid diethyl ether complex or trifluoroacetic acid solutions resulted in deep orange monocation **11-H$^+$** formation in the first stage, followed by red-brown dication **11-H$_2^{2+}$** (Scheme 3).

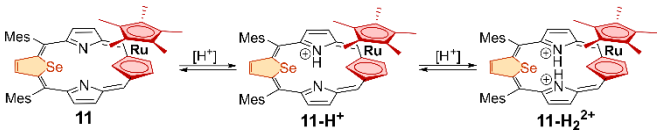

Scheme 3. Protonation of **11**.

The protonation of both pyrrole nitrogen atoms resulted in the relocation of the H(2,3) and H(21) ^{1}H NMR signals to 5.87 and 1.76 ppm in **11-H$_2^{2+}$**, respectively (Figure 7d). The signals of meso, selenophene, and pyrrole hydrogens show downfield transfer to 8.66, 8.03, 8.19, and 7.32 ppm, correspondingly, due to aromatic current amplification. Symmetry lowering of **11-H$^+$** due to the protonation of one pyrrole nitrogen atom is reflected in the ^{1}H NMR spectrum (Figure 7c). The UV/Vis electronic spectra of **11-H$^+$** and **11-H$_2^{2+}$** are shown in Supporting Information (Figure S29).

The ^{1}H NMR spectra of the palladium(II) complexes of 21-carbaselenaporphyrinoids **12**, **13**, and **14** exhibit resonances at positions consistent with their aromatic structures (Figures 8a, S10, and S15). The bonding of the $[RuCp^*]^+$ cation to the cyclopentadiene ring of **14** resulted in the formation of two isomers of a bimetallic complex (**15-A** and **15-B**, Scheme 2). These isomers are differentiated by the orientation of the selenophene ring, which is tilted toward or against the $[RuCp^*]^+$ moiety in **15-A** and **15-B**, respectively. At 300 K, both stereoisomers of **15** exhibit well-separated sets of ^{1}H NMR resonances with similar patterns (Figure 8b). Each set of signals was assigned to a specific isomer based on the GIAO-calculated ^{1}H NMR spectra for the DFT-optimized structures (Figures S23, S41, and S42). The ratio of **15-A** to **15-B** isomers, determined through the analysis of ^{1}H NMR spectra, is 1:0.7 (300 K). The external meso (H(5,20)), pyrrole (H(7,18); H(8,17)), selenophene (H(12,13)), and cyclopentadiene (H(2,3)) protons exhibit resonances that are shifted upfield relative to the parent **14** (Figure 8a) indicating a weakening of the aromatic ring current due to coordination of the $[RuCp^*]^+$ moiety.

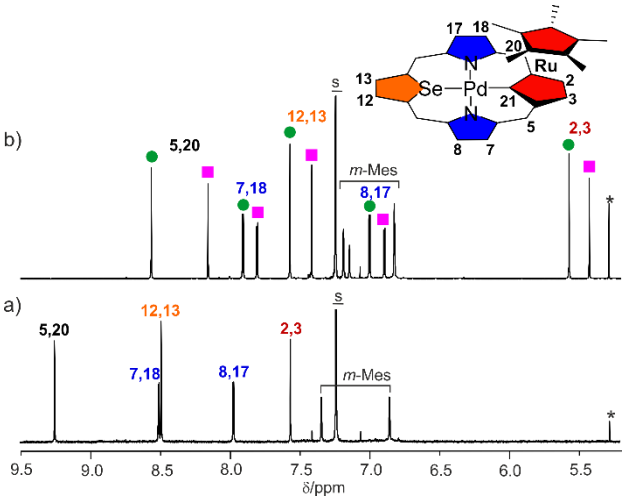

Figure 8. ^{1}H NMR spectra for compounds a) **14** and b) two isomers of **15** (**15-A** denoted as green circles, **15-B** denoted as pink squares; 300 K, [D]chloroform). *o*,*p*-Methyl range is omitted (see SI for details).

A rare example of stereoselective porphyrin metalation[24] was encountered once ruthenocenoporphyrin **11** was engaged as a macrocyclic ligand. Thus, the reaction with $PdCl_2$ resulted in the selective formation of a single stereoisomer of **15**, presumably **15-B**, due to the steric hindrance imparted by the $[RuCp^*]^+$ fragment (Scheme 2). A feasible conversion to the counterpart was not detected in [D]chloroform (300 K) over 48 hours, as followed by ^{1}H NMR spectroscopy.

A density functional theory (DFT) study was conducted for complexes **11** and **15** to elucidate the electronic structure of the 21-carbaselenaporphyrin and its palladium(II) complex following π-coordination of the cyclopentadienyl ring to the $[RuCp^*]^+$ moiety.

A comparison of the crystal and DFT-optimized structures of **11** reveals a high degree of agreement. This is evidenced by a detailed comparison of the bond lengths, as shown in Figures S35 and S36. Both isomers of **15** were subjected to DFT studies and the final geometries are presented in Figure 9. The triheterocyclic braces involving two pyrrole and cyclopentadienyl rings demonstrate planar geometry. In contrast, selenophene is tilted from the macrocyclic plane. The geometry of the transient species **15-t$_0$** with the selenophene ring located in the carbaporphyrinic plane was also considered. The selenophene tilt angles from the four *meso*-carbon atoms plane equal −37.2° (**15-A$_0$**) and 35.3° (**15-B$_0$**), for the transient species **15-t$_0$** is close to 0°. The energy difference between isomers **15-A** and **15-B** is negligible (ΔE = 0.5 kcal/mol). The transient form **15-t$_0$**, with the selenophene ring in the macrocyclic plane, has much higher energy than **15-B$_0$**, with the barrier of 34.0 kcal/mol.

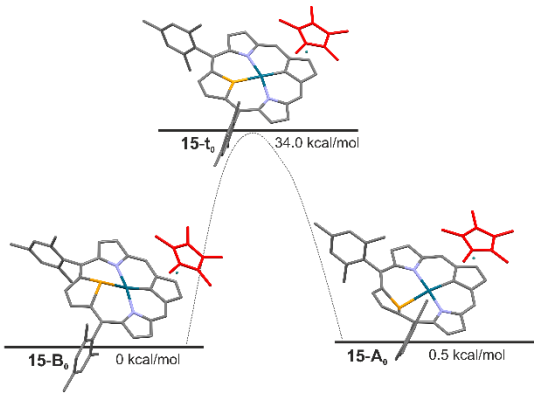

Figure 9. Energy diagram for conformational interconversion of **15**. Provided are calculated relative energy differences.

The aromaticity of the carbaselenaporphyrin unit has been analyzed in detail after the coordination of the [RuCp*]$^+$ cation to cyclopentadiene ring in **11** and **15**. The significant resonance contributors for carbaselenapophyrin anion in **11**, involving the delocalization of 18 π-electrons (**11-A**) or 6 π-electrons (**11-B**) within a cyclopentadienyl ring are shown in Scheme 4. The magnetic properties of π-complex **11** can be considered as a result of a hard-fought struggle for the supremacy of global vs. local aromatic delocalization encompassed in resonance structures **11-A** vs. **11-B**.

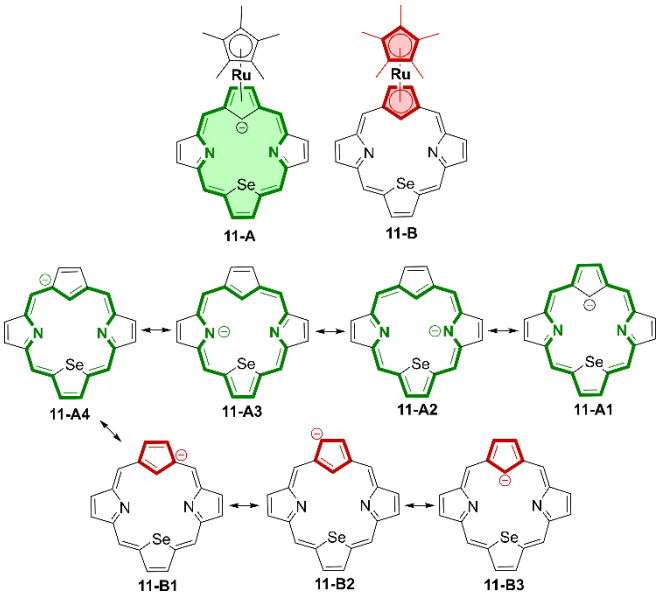

Scheme 4. Resonance structures of the **11** anion.

The comparison of bond lengths in the DFT-optimized geometries of the selenatripyrrin fragment of **11** and **9-I** indicates a strong bond equalization in the aromatic 21-carbaselena-porphyrin **9-I** (Figure S37). Conversely, a significant alternation in bond lengths is observed in **11** after coordination of the [RuCp*]$^+$ fragment, due to a less efficient π delocalization effect.

The electron density of delocalized bonds (EDDB)[25] was employed to investigate cyclic π delocalization across conjugated bonds in **11** and **15**, with **9** and **14** serving as comparative controls (Figures 10a-c and S38). The EDDB isocontour maps of **11** and **11-H$_2^{2+}$** reveal the presence of localized π-conjugation on the cyclopentadienyl ring, which does not disrupt the π delocalization throughout the carbaporphyrin structure (Figures 10b and 10c). It is observed that effective π-conjugation occurs through the 1,3-substituted ruthenocene moiety.

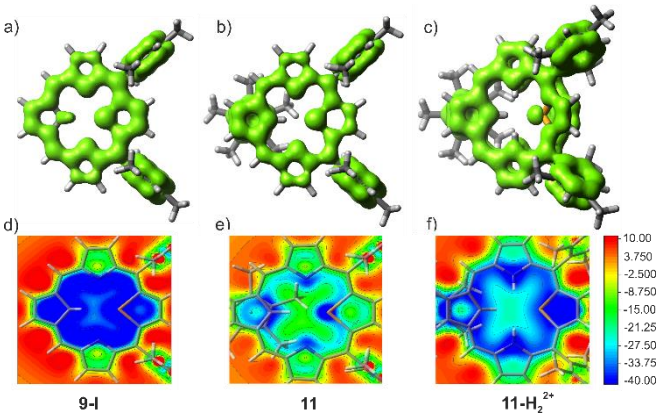

Figure 10. EDDB plots (a-c) and NICS(1)zz 2D maps (d-f) of 21-carba-23-selenaporphyrin **9-I** (a,d), ruthenium(II) π complex **11** (b,e), and **11-H$_2^{2+}$** (c,f). In EDDB plots the localized and delocalized cyclic π-conjugation is shown with the green surface with an isovalue of 0.014, while NICS maps are estimated 1 Å above the mean plane. RuCp* located behind the carbaporphyrinic plane.

The aromaticity of ruthenocenoselenaporphyrin **11** and its dication **11-H$_2^{2+}$** was further analyzed using nucleus-independent chemical shifts (NICS) calculations.[26] The analysis of the NICS 2D map of **11** revealed negative values within the inner cavity of the macrocyclic ring (Figure 10e). However, these values were significantly less negative than those observed for the control **9-I** (Figure 10d). After protonation in **11-H$_2^{2+}$**, the aromaticity features became more visible (Figure 10f). The NICS(0) values were calculated for molecules **11** and **11-H$_2^{2+}$** at the centers of macrocycles (Figure S34). After binding of the [RuCp*]$^+$ moiety to **9**, the corresponding NICS(0) values are noticeably less negative −8.5 in **11** and −10.0 in **11-H$_2^{2+}$** compared to **9** (−16.7 in **9-I**, −14.8 in **9-II**).

These observations are consistent with the ^{1}H NMR spectroscopic patterns and the electronic absorption spectra (decreasing molar absorption coefficient). The differences in the efficiency of π-delocalization in 21-carba-23-selenaporphyrin **9-I**, ruthenocenoselenaporphyrin **11**, and its dication **11-H$_2^{2+}$** are readily apparent in NICS 2D maps. The EDDB contour plots and NICS 2D maps both demonstrate the π-delocalization across the 1,3-ruthenocene fragment. Analogous observations have been made for the bimetallic complex **15** and the control palladium complex **14** (Figure S38). However, in this particular case, the strong deviation of the selenophene ring from the macrocyclic

plane defined by the *meso*-carbon atoms contributes to a decrease in the π-conjugation efficiency.

^{1}H and ^{13}C NMR chemical shifts calculated for **11**, **11-H$_2^{2+}$**, **15-A**, and **15-B** are presented in the Supporting Information (Tables S3-S6). The theoretical results correlate well with the experimental shifts obtained from ^{1}H and ^{13}C NMR spectroscopy, except for the upfield relocated inner proton H(21) in **11** and **11-H$_2^{2+}$** (Figures S39 and S40) and C(21) in **15** (Figures S41 and S42).

Conclusion

In conclusion, the π coordination of the [RuCp*]$^{+}$ fragment to the cyclopentadienyl ring incorporated into the 21-carba-23-selenaporphyrin was developed. Consequently, the incorporation of ruthenocene subunits at the 1,3-positions into fully π-delocalized macrocycle – 21-carbaselenaporphyrin led to the formation of a hybrid molecule – aromatic ruthenocenoselenaporphyrin. The evidence for direct transmission of π-electron conjugation across a *d*-electron ferrocene or ruthenocene was previously provided by the exploration of ferroceno- and ruthenocenoporphyrinoids incorporating 1,1'-metallocene. The present work reveals a hitherto unknown feature of metallocenoporphyrinoids. The relevant ^{1}H NMR spectra of ruthenocenoselenaporphyrin and its protonated forms confirmed the presence of macrocyclic aromaticity. The aromaticity and π-delocalization patterns were visualized using EDDB plots and NICS 2D maps. Remarkably, ruthenocenoselenaporphyrin acts as a monoanionic organometallic macrocyclic ligand, as evidenced by the formation of a heterometallic ruthenium(II)-palladium(II) derivative, providing the rear example of M–C σ-coordination of the metallocene unit in the macrocyclic surroundings.

Further investigation into macrocyclic organometallic chemistry may entail the synthesis of analogous metallocenoporphyrins utilizing a range of metallocenes and 21-carba-23-heteroporphyrins as fundamental building subunits. The feasible interplay between two metal cations locked in the firm molecular architecture offers a novel route for organometallic and metallocene-focused investigations, combining the benefits of metallocene and carbaporphyrin strategies.

Supporting Information

The authors have cited additional references within the Supporting Information.[27-37] Data for this article, including NMR spectra, are available at ZENODO at doi.org/10.5281/zenodo.14099129. The remaining data have been included in the Supplementary Information.

Acknowledgements

Financial support from the National Science Center (Grant 2016/23/B/ST5/00161 of L. L.-G., Grant 2020/39/D/ST4/00021 of M.J.B) is kindly acknowledged. DFT calculations were carried out using resources provided by the Wrocław Centre for Networking and Supercomputing Grant no. 329.

Keywords: aromaticity • carbaporphyrin • π-delocalization • metallocene • ruthenocenoporphyrin

[1] a) M. Stępień, N. Sprutta, L. Latos-Grażyński, *Angew. Chem. Int. Ed.* **2011**, *50*, 4288□4340; b) A. Osuka, S. Saito, *Chem. Commun.* **2011**, *47*, 4330□4339; c) D. Sundholm, H. Fliegl, in *Handbook of Porphyrin Science* (Eds.: K.M. Kadish, K.M.G.R., Smith), **2022**, pp. 1–39; d) M. Toganoh, H. Furuta, *Chem. Commun.* **2012**, *48*, 937–954.

[2] I. Simkowa, L. Latos-Grażyński, M. Stępień, *Angew. Chem. Int. Ed.* **2010**, *49*, 7665–7669.

[3] I. Grocka, L. Latos-Grażyński, M. Stępień, *Angew. Chem. Int. Ed.* **2013**, *52*, 1044–1048.

[4] K. Miwa, T. Yokota, Q. Wang, T. Sakurai, H. Fliegl, D. Sundholm, H. Shinokubo, *J. Am. Chem. Soc.* **2024**, *146*, 1396–1402.

[5] N. Halder, K. C. Sahoo, K. Gourav, D. Usharani, H. Rath, *J. Org. Chem.* **2021**, *86*, 8015–8026.

[6] a) S. Ramakrishnan, K. S. Anju, A. P. Thomas, E. Suresh, A. Srinivasan, *Chem. Commun.* **2010**, *46,* 4746–4748; b) N. Halder, M. Jana, S. Kottekad, D. Usharani, H. Rath, *Chem. Asian. J.* **2022**, *17*, e202200108; c) T. Chatterjee, G. G. Theophall, K. I. Silva, K. V. Lakshmi, M. Ravikanth, *Inorg. Chem*. **2016**, *55*, 6873–6881; d) J. Qu, Y. Song, W. Ji, S. Jing, D. Zhu, W. Huang, M. Zheng, Y. Li, J. Ma, *Dalton Trans.* **2016**, *45*, 3417–3428.

[7] a) C. P. Villamizar C, P. Sharma, B. Anzaldo, R. Gonzalez, R. Gutierrez, A. Kumar, *Polyhedron* **2022**, *227*, 116081–116091; b) N. Singh, A. J. Elias, *Organometallics* **2012**, *31*, 2059–2065; c) P. Gupta, S. Madhavan, M. Kapur, *Angew. Chem. Int. Ed.* **2023**, *62*, e202305278.

[8] A. Vecchi, P. Galloni, B. Floris, S. V. Dudkin, V. N. Nemykin, *Coord. Chem. Rev.* **2015**, *291*, 95–171.

[9] L. Cuesta, J. L. Sessler, *Coord. Chem. Rev.* **2009**, *38*, 2716–2729.

[10] L. Cuesta, E. Karnas, V. M. Lynch, J. L. Sessler, W. Kajonkijya, W. Zhu, M. Zhang, Z. Ou, Karl. M. Kadish, K. Ohkubo, S. Fukuzumi, *Chem. Eur. J.* **2008,** *14*, 10206–10210.

[11] L. Cuesta, E. Karnas, V. M. Lynch, P. Chen, J. Shen, K. M. Kadish, K. Ohkubo, S. Fukuzumi, J. L. Sessler, *J. Am. Chem. Soc.* **2009**, *131*, 13538–13547.

[12] A. Nakai, S. Ishida, T. Soya, A. Osuka, *Angew. Chem. Int. Ed.* **2019**, *58*, 8197–8200.

[13] H. J. H. Wang, L. Jaquinod, D. J. Nurco, M. G. H. Vicente, K. M. Smith, *Chem. Commun.* **2001**, *1*, 2646–2647.

[14] M. Toganoh, H. Matsuo, A. Sato, H. Furuta, *Chem. Eur. J.* **2016**, *22*, 8316–8322.

[15] T. Yamamoto, K. Mitsuno, S. Mori, S. Itoyama, Y. Shiota, K. Yoshizawa, M. Ishida, H. Furuta, *Chem. Eur. J.* **2018**, *24*, 6742–6746.

[16] A. Berlicka, P. Foryś-Martowłos, M. J. Białek, K. Stasiak, A. Walczak, A. Wójcik, A. Białońska, L. Latos-Grażyński, *Angew. Chem. Int. Ed.* **2024**, 63, e202314925.

[17] A. Berlicka, P. Dutka, L. Szterenberg, L. Latos-Grażyński, *Angew. Chem. Int. Ed.* **2014**, *53*, 4885‑4889.

[18] A. Berlicka, P. Foryś-Martowłos, K. Hassa, M. J. Białek, K. Ślepokura, L. Latos-Grażyński, Org. Chem. Front. **2022**, *9*, 5440–5452.

[19] M. Garbicz, L. Latos-Grażyński, *Angew. Chem. Int. Ed.* **2019**, *58*, 6089–6093.

[20] Deposition numbers 2400821 (for **11**), and 2400822 (for **13**) contain the supplementary crystallographic data for this paper. These data are

provided free of charge by the joint Cambridge Crystallographic Data Centre and Fachinformationszentrum Karlsruhe Access Structures service.

[21] M. Rioja, P. Hamon, T. Roisnel, S. Sinbandhit, M. Fuentealba, K. Letelier, J. Y. Saillard, A. Vega, J. R. Hamon, *Dalton Trans.* **2015**, *44*, 316–329.

[22] M. Watanabe, H. Sano, *Org. Lett.* **1991**, 555–558.

[23] K. N. Seneviratne, A. Bretschneider-Hurley, C. H. Winter, *J. Am. Chem. Soc.* **1996**, *118*, 5506–5507.

[24] S. Le Gac, B. Najjari, V. Dorcet, T. Roisnel, L. Fusaro, M. Luhmer, E. Furet, J.-F. Halet, B. Boitrel, *Chem. Eur. J*., **2013**, *19*, 11021–11038.

[25] a) B. Basumatary, H. Tsuruda, D. W. Szczepanik, J. Lee, J. Ryu, S. Mori, K. Yamagata, T. Tanaka, A. Muranaka, M. Uchiyama, J. Kim, M. Ishida, H. Furuta, *Angew. Chem. Int. Ed.* **2024**, *63*, e202405059; b) H. He, J. Lee, Z. Zong, J. Kim, V. M. Lynch, J. Oh, D. Kim, J. L. Sessler, X.-S. Ke, *Nat. Commun.* **2024**, 15, 2913–2923; c) T. M. Krygowski, M. K. Cyrański, *Chem. Rev.* **2001**, *101,* 1385–1420.

[26] P. von Ragué Schleyer, C. Maerker, A. Dransfeld, H. Jiao, N. J. R. van Eikema Hommes, *J. Am. Chem. Soc.* **1996,** *118,* 6317–6318.

Entry for the Table of Contents

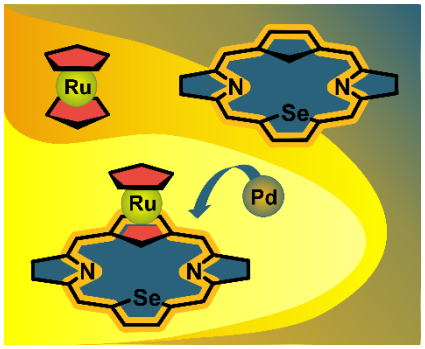

The coordination of the $[RuCp^*]^+$ moiety to the cyclopentadienyl π-surface of 21-carba-23-selenaporphyrin or its palladium(II) complex resulted in the formation of original molecular hybrids incorporating 1,3-ruthenocene fragment. The NICS 2D maps and EDDB plots visualize the aromaticity and π-conjugation in the ruthenocenoselenaporphyrin.

Institute and/or researcher Twitter usernames: @AnnaBerlicka, @Supermolecule01